Global Modeling and Assimilation Office

GMAO Office Note No. 5 (Version 1.0)

Model Configuration for the 7-km GEOS-5 Nature Run, Ganymed Release

Non-hydrostatic 7 km Global Mesoscale Simulation

Release Date: 10/28/2014

Global Modeling and Assimilation Office
Earth Sciences Division
NASA Goddard Space Flight Center
Greenbelt, Maryland 20771

This page intentionally left blank.

Model Configuration for the 7-km GEOS-5 Nature Run, Ganymed Release

Non-hydrostatic 7 km Global Mesoscale Simulation

Document maintained by William Putman and Arlindo da Silva (GMAO, NASA/GSFC)

This document should be cited as:

Approved by:

_____   October 28, 2014

Steven Pawson   Date

Chief, Global Modeling and Assimilation Office
Code 610.1, NASA GSFC

REVISION HISTORY

Version	Revision Date	Extent of Changes
1.0	10/28/2014	Baseline

Table of Contents

This page intentionally left blank.

1. Introduction

The most recent version of the GEOS-5 Atmospheric General Circulation Model (GEOS-5 AGCM) uses the non-hydrostatic finite-volume dynamics (an extension of Lin, 2004) integrated with various physics packages (e.g., Bacmeister et al., 2006), under the Earth System Modeling Framework (ESMF, Hill *et al.,* 2004) including the Catchment Land Surface Model (CLSM) (*e.g*., Koster *et al*., 2000). The GEOS-5 AGCM is documented in Rienecker *et al*. (2008) with more recent updates described in Molod *et al*. (2011).

This document describes the specific GEOS-5 model configuration used to perform a two-year global, non-hydrostatic mesoscale simulation for the period 2005-2007 at 7-km horizontal resolution. Because this simulation is intended to serve as a reference *Nature Run* for Observing System Simulation Experiments (OSSEs, e.g., Errico *et al.*, 2012) it will be referred to as the *7-km GEOS-5 Nature Run or 7-km G5NR*. This simulation has been performed with the Ganymed version of GEOS-5, more specifically with CVS Tag *wmp-Ganymed-4_0_BETA8*.

In addition to standard meteorological parameters (wind, temperature, moisture, surface pressure), this simulation includes 15 aerosol tracers (dust, sea-salt, sulfate, black and organic carbon), O_3, CO and CO_2. This model simulation is driven by prescribed sea-surface temperature and sea-ice, as well as surface emissions and uptake of aerosols and trace gases, including daily volcanic and biomass burning emissions, biogenic sources and sinks of CO_2, and high-resolution inventories of anthropogenic sources.

The simulation is performed at a horizontal resolution of 7 km using a cubed-sphere horizontal grid with 72 vertical levels, extending up to 0.01 hPa (~ 85 km). For user convenience, all data products are generated on two logically rectangular longitude-latitude grids: a *full-resolution* 0.0625^o grid that approximately matches the native cubed-sphere resolution, and another 0.5^o *reduced-resolution* grid. The majority of the full-resolution data products are instantaneous with some fields being time-averaged. The reduced-resolution datasets are mostly time-averaged, with some fields being instantaneous. Hourly data intervals are used for the reduced-resolution datasets, while 30-minute intervals are used for the full-resolution products. All full-resolution output is on the model's native 72-layer vertical grid, while the reduced-resolution output is given on both the native vertical levels and on 42 pressure surfaces extending up to 0.1 hPa. GMAO Office Note 6 (da Silva *et al.*, 2014) presents additional details on horizontal and vertical grids.

The GEOS-5 Nature Run data products are organized into file collections that are described in detail in da Silva and Putman (2014). Additional details about variables listed in this file specification can be found in a separate document, the *GEOS-5 File Specification Variable Definition Glossary.* Documentation about the current access methods for products described in this document can be found on the GMAO products page: http://gmao.gsfc.nasa.gov/products/ .

This document is organized as follows. Section 2 gives an overview of the ESMF component-based architecture adopted in GEOS-5. The cubed-sphere atmospheric dynamics is summarized in Section 3, while information on the specific model parameterizations are given in Section 4. The treatment of atmospheric aerosols is explained in Section 5, followed by a description of the relevant parameterizations used for representing CO and CO_2 carbon species in Section 6. Finally, Section 7 describes the main boundary conditions and external datasets utilized in this simulation.

2. GEOS-5 Software Architecture

2.1 The ESMF Foundation

The Earth System Modeling Framework (ESMF) is a high-performance, flexible software infrastructure to increase ease of use, performance portability, interoperability, and reuse in climate, numerical weather prediction, data assimilation, and other Earth science applications. The ESMF project was initiated by NASA in 2002 and, over the last decade, it has become a widely used tool in the Earth Sciences. Models that have implemented ESMF interfaces include the current GEOS-5 Earth System model, the Community Earth System Model (CESM), the Weather Research and Forecast model (WRF), NOAA's National Environmental Modeling System (NEMS), Naval Research Laboratory's Coupled Ocean-Atmosphere Mesoscale Prediction System (COAMPS), and the GFDL Modular Ocean Model (MOM4).

The ESMF defines a component-based architecture for composing complex, coupled modeling systems and includes data structures and utilities for developing individual models. It includes high-performance software for representing and coupling model components, and a set of utilities for common modeling functions. ESMF is implemented as a collection of very general programming classes that can be used both to construct ESMF components and to connect them to one another. These classes thus support modelers in building interoperable and portable codes. This design is illustrated by the ESMF sandwich

Figure 1. The ESMF sandwich diagram, illustrating the relationship between the ESMF architecture and the user's computational code.

diagram (Figure 1), where the user's computational code sits between the two ESMF layers. In general, componentization with ESMF has been implemented at the level of major physical domains, where simulated interactions require inter-component data communications (e.g., atmosphere, ocean), and has been implemented as wrappers that minimally modify existing user code.
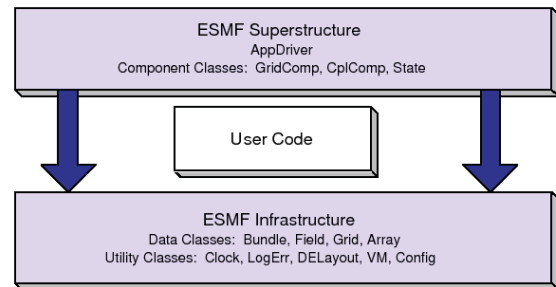
2.2 MAPL: A Toolkit for building ESMF Compliant Applications

As the ESMF became available, several groups were involved in prototyping its use in climate and weather prediction models and in data assimilation systems. Comparing the various implementations led to two seemingly contradictory conclusions: all implementations are different and much of what they do is the same. Both conclusions were anticipated, since ESMF is a general framework designed to meet a wide variety of needs. This generality is an important strength of the ESMF design, but it also implies that there are many different ways of using ESMF – even when performing very similar tasks.

The Modeling Analysis and Prediction Layer (MAPL) software library (Suarez et al., 2014) arose as a response to this early experience, particularly during the construction of GEOS-5.   MAPL is based on the observation that much of the work done in these initial implementations can be standardized; thus, reducing the labor of constructing ESMF applications, as well as increasing their interoperability. MAPL provides:

- Specific conventions and best practices for the utilization of ESMF in climate models
- A middle-ware software layer (between the model and ESMF) that facilitates the adoption of

ESMF by climate models.

A MAPL-based component is a fully compliant ESMF component that accesses the MAPL library to build and execute. The parent code in an application that uses a MAPL-based component is not required to use the MAPL machinery for coupling. For example, the MAPL-based GOCART aerosol component is implemented in NOAA's National Environmental Modeling System (NEMS), but NEMS itself does not use any of the MAPL coupling capabilities.

The NUOPC (http://www.earthsystemmodeling.org/nuopc/NUOPC_refdoc/) layer provides similar functionality for coupling high-level components such as oceanic and atmospheric models. In contrast, MAPL is designed to hierarchically couple components at a much higher level of granularity, from physical parameterizations all the way to components that represent the full climate system.

2.3 Overview of GEOS-5 Components

Unlike other models that use the ESMF at the very high level to couple "model components" (ocean, atmosphere, etc.), GEOS-5 relies on the infrastructure provided by MAPL to couple atmospheric dynamics, radiation, moist processes, ocean and land surface, chemistry and aerosol processes, etc. Figure 2 illustrates the hierarchical organization of grid components in the version[1] of the GEOS-5 AGCM used to perform the 7-km G5NR.
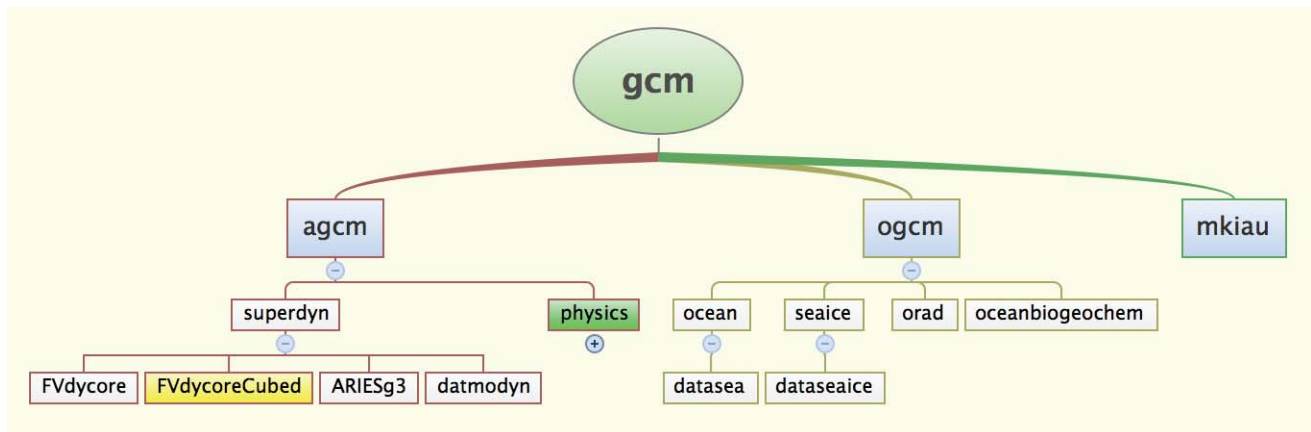

Figure 2. Part of the hierarchical structure of the ESMF grid components in GEOS-5. This diagram was automatically generated from the GEOS-5 source code used for the Nature Run.

The three main components are the atmospheric GCM (*agcm*), the oceanic GCM (*ogcm*), and the data assimilation related component (*mkiau*) which is not active in this simulation). Notice that the G5NR was performed with prescribed sea surface temperature and sea ice (*datasea* and *dataseaice*). Among the several choices of dynamics, G5NR was run with the Finite-volume dynamics on the cubed-sphere grid (*FVdycoreCubed*). The breakdown of the *physics* component appears in Fig. 3, showing the parameterization of moist processes (*moist*), *surface* processes, *radiation*, *turbulence*, *chemistry* and gravity wave drag (*gwd*). While this system provides several chemistry options, G5NR was run with *GOCART* aerosols (the CO and CO_2 tracers are also embedded in the GOCART ESMF module) and the Parameterized Chemistry (*pchem*) component. The Chemistry component (*chem)* provides aerosols, ozone and other radiatively active gases for the *radiation* parameterization. Additional information on these components are given below.

---

[1] Specifically, this system is based on module Ganymed with CVS Tag *wmp-Ganymed-4_0_BETA8*.
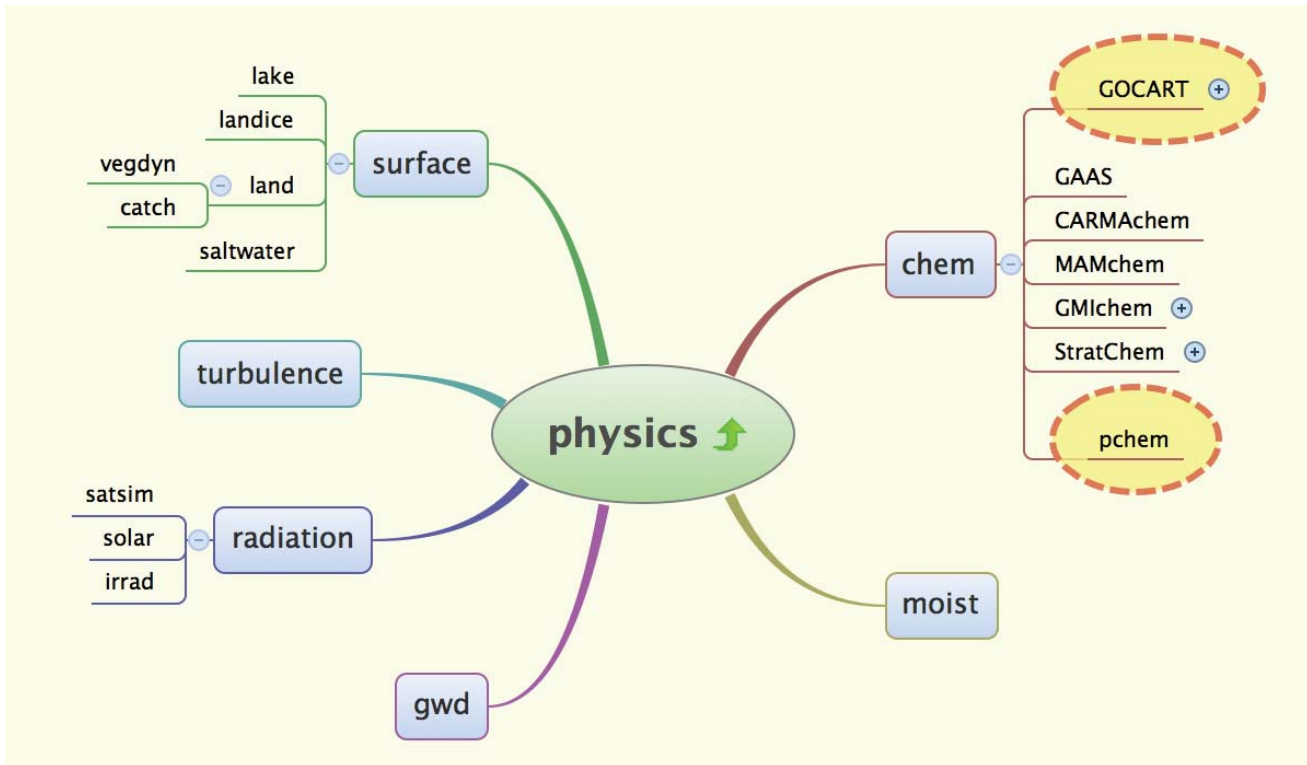
Figure 3. The hierarchical structure of the GEOS-5 physics component and its children in the ESMF framework. This diagram highlights the modular nature of the different physical process components in GEOS-5, including the adoption of the GOCART chemistry package, and other chemical modules (GAAS, CARMAchem, MAMchem, GMIchem, StratChem) that are options not invoked in the 7-km G5NR simulation.

3. Atmospheric Dynamics

The *finite-volume (FV) dynamics* utilized within GEOS-5 evolved from a foundation of multi-dimensional flux-form schemes from Gudunov (1959) and Van Leer (1977), using higher order sub-grid schemes with the introduction of the "piecewise parabolic method" of Woodward and Colella (1981). These methods were generalized to multi-dimensional schemes for global atmospheric modeling within the FV dynamics (Lin and Rood, 1996).

The flux-form scheme consists of a two-grid approach under the shallow water framework for consistent transport of mass and absolute vorticity. A split-explicit time-stepping approach is applied to produce a fully explicit shallow water scheme with sufficient computational efficiency (Lin and Rood, 1997). The pressure gradient term follows a finite-volume approach in terrain following coordinates (Lin 1997, 1998), using a Lagrangian control-volume vertical coordinate (Lin and Rood 1998, 1999) simplifying the 3-dimensional scheme to a series of stacked 2-dimensional shallow water layers, periodically remapped to an Eulerian terrain-following coordinate with a mass, momentum, and total energy conserving algorithm (Lin, 2004).

The original FV algorithm (Lin, 2004), designed for orthogonal coordinate systems, has been extended to operate in a general curvilinear coordinate system on the cubed-sphere grid (Putman and Lin, 2007, 2009), with explicit treatment of edge discontinuities at intersecting faces of the cubed-sphere grid. The cubed-sphere FV dynamics also includes an improved piecewise-parabolic method (PPM) for construction of sub-grid distributions in the advection scheme with the addition of Huynh's 2nd constraint (Huynh, 1996) for monotonicity.

4

One of the most unique aspects of the hydrostatic FV dynamics is its use of the terrain-following Lagrangian coordinate system (Lin, 2004). The improved accuracy in vertical transport characteristics relative to commonly used cores, such as the spectral core, has been documented by Rasch et al. (2006). At cloud-permitting resolution (1-15 km), the vertical velocity can become very large (~30 m/s updrafts are not uncommon with ~3-10 km resolution). The use of a Lagrangian coordinate system, as in the FV dynamics, removes this potentially severe time-step restriction without ad hoc vertical-velocity damping.

The hydrostatic formulation of Lin (2004) has been extended to the fully compressible non-hydrostatic flow (essentially the unapproximated Euler equations on the sphere). To maintain the advantages of the "vertically Lagrangian discretization" of the hydrostatic system, an explicit sound wave solver based on the conservation of Riemann invariants was developed. Due to the vertical CFL condition imposed by the vertically propagating sound waves, traditional "Riemann solvers" available in the literature require the use of a prohibitively small time step (e.g., Carpenter *et al.*, 1990). The Riemann solver we developed for the non-hydrostatic FV dynamics is consistently "Lagrangian," in the sense that contributions from all the sound waves within the entire physical domain of dependence are considered, not just the two nearby volumes, as in typical finite-volume CFD (computational fluid dynamics) solvers. As a result, the time step is not severely limited by the vertically propagating sound waves: the model runs stably with sound-wave Courant numbers up to 100.

The 7-km G5NR is executed with a heartbeat time step of 300 seconds. This heartbeat is the time step at which the physics and dynamics components are called during execution. The FV dynamics further sub-cycles this time step for CFL stability, executing at a small time step of five seconds while remapping the Lagrangian vertical coordinate back to the Eulerian terrain-following coordinates every 75 seconds. A vertical sponge layer is included in the FV formulation to damp the top layers and prevent reflection of vertically propagating waves off of the model top from contaminating the simulation. This sponge layer is applied to the top two model levels with an increased amplitude of second order horizontal diffusion applied to these layers.

4. Model Physics: Parameterizations

The GEOS-5 AGCM physics includes parameterization schemes for atmospheric convection, large-scale precipitation and cloud cover, longwave and shortwave radiation, turbulence, gravity wave drag, a land surface model, and a simple glacier model. These physics parameterizations are scale aware, in that they dynamically adapt to the horizontal resolution of GEOS-5 (as described in the text). This multi-scale design allows GEOS-5 to easily move from climate simulations on the order of 50- to 100-km resolutions, to medium range weather prediction and data assimilation resolutions of 25-km, to cloud permitting resolutions of 14- to 3.5-km (Putman and Suarez, 2011).

Convection is parameterized using the Relaxed Arakawa-Schubert (RAS) scheme of Moorthi and Suarez (1992) and includes a scheme for the generation and re-evaporation of falling rain (Bacmeister *et al*., 2006). RAS is a mass flux scheme with an updraft-only detraining plume cloud model and a quasi-equilibrium closure. As resolution is increased, the convection parameterization is restrained using a stochastic, resolution-dependent limit on deep convection (Tokioka et al., 1988). As resolution increases approaching cloud resolving scales (15- to 1-km), the large-scale moist processes begin to explicitly resolve some of the deep convection. This stochastic limiting scheme essentially prevents deep convection and restricts RAS to act as a shallow convection scheme. For the 7-km G5NR, this limiting parameter (MAXDALLOWED) is set to 450. Additionally, the RAS scheme is constrained by the choice of shallow and deep convective time-scales: the longer the time-scale, the more restrained RAS becomes. In the 7-km G5NR these time-scales (RASAL1 and RASAL2) are set to 1800 and 43200 seconds for shallow and deep convection respectively.

The prognostic cloud cover and cloud water and ice scheme is from Bacmeister et al. (2006), with the

total water probability distribution function (pdf) of Molod (2012). The critical relative humidity within the pdf increases as the grid cell area shrinks, for the 7-km G5NR this parameter (MINRHCRIT) is set to 0.98. The scheme includes large-scale condensation, evaporation, autoconversion and accretion of cloud water and ice, sedimentation of cloud ice and re-evaporation of falling precipitation.

As in the GEOS-5 configuration described in Rienecker *et al*. (2008), the longwave radiative processes are described by Chou and Suarez (1994), and include absorption due to cloud water, water vapor, carbon dioxide, ozone, nitrous oxide and methane. The shortwave radiation transfer module is from Chou (1990) and Chou (1992), and includes absorption by water vapor, ozone, carbon dioxide, oxygen, cloud water, and aerosols and includes scattering by clouds water and aerosols.

The turbulence parameterization is based on the Lock *et al*. (2000) scheme, acting together with the Richardson-number-based scheme of Louis and Geleyn (1982). The Lock scheme includes a representation of non-local mixing (driven by both surface fluxes and cloud-top processes) in unstable layers, either coupled to or decoupled from the surface. The original scheme was extended in GEOS-5 to include moist heating and entrainment in the unstable surface parcel calculations. The Monin-Obukhov similarity theory based parameterization of surface layer turbulence is described in Helfand and Schubert (1995), and includes the effects of a viscous sublayer for heat and moisture transport over all surfaces except land. The ocean roughness is determined by a blend of the algorithms of Large and Pond (1981) and Kondo (1975), modified in the mid-range wind regime according to Garfinkel *et al*. (2011) and in the high wind regime according to Molod *et al*. (2013).

The gravity wave parameterization computes the momentum and heat deposition into the grid-scale flow due to orographic (McFarlane, 1987) and nonorographic (after Garcia and Boville, 1994) gravity wave breaking. Mountain waves are forced by the sub-grid orographic variability, the variance of the orography is scaled down with increasing resolution to account for the better resolved topographically induced gravity waves due to increased resolution in the dynamics. This variance is controlled by model parameter (EFFGWORO) which is set to 0.015625 in the 7-km GEOS-5 Nature Run. The smallest scales (< 10km) are not used to force gravity waves, but enter into an orographic form drag used in the turbulence module.

The Land Surface Model from Koster *et al*. (2000) is a catchment-based scheme which treats subgrid-scale heterogeneity in surface moisture statistically. The applied subgrid-scale distributions are related to the topography, allowing it to exert a major control over much of the subgrid variability. For glaciated land, the surface is represented with a 15-layer ice column for the conduction of heat below the snow-ice interface (Cullather *et al*., 2014), while the overlying snow cover is allowed to be fractional. The catchment and glacier models are each coupled to the multi-layer snow model of Stieglitz *et al*. (2001). Southern Hemisphere sea ice albedo is prescribed to be 0.6, while Northern Hemisphere sea ice albedo varies on the annual cycle based on observed values (Duynkerke and de Roode, 2001).

5. Atmospheric Aerosols

A version of the Goddard Chemistry, Aerosol, Radiation, and Transport model (GOCART, Chin *et al*., 2002) is run online, with coupling to the GEOS-5 radiation code (Colarco *et al*., 2010). GOCART treats the sources, sinks, and chemistry of dust, sulfate, sea salt, and black and organic carbon aerosols. Aerosol species are assumed to be external mixtures. Total mass of sulfate and hydrophobic and hydrophilic modes of carbonaceous aerosols are tracked, while for dust and sea salt the particle size distribution is explicitly resolved across five non-interacting size bins for each. Both dust and sea-salt have wind-speed dependent emission functions, while sulfate and carbonaceous species have emissions principally from fossil fuel combustion, biomass burning, and biofuel consumption, with

additional biogenic sources of organic carbon. Sulfate has additional chemical production from oxidation of SO_2 and DMS, and we include a database of volcanic SO_2 emissions and injection heights. Details about the specific emission datasets are given in Section 7.

For all aerosol species, optical properties are primarily from the commonly used OPAC data set (Hess *et al*. 1998). We have recently updated our dust optical properties data set to incorporate non-spherical dust properties based on Meng et al. (2010), which permits, for example, calculation of the aerosol depolarization ratio. Stratospheric aerosol perturbations and their chemical, radiative, and dynamical impacts in GEOS-5 have been studied in the context of volcanic eruptions (Aquila *et al*. 2012, 2013, 2014), geo-engineering (Pitari *et al*., 2014), and meteor inputs (Gorkavyi *et al*., 2013). The GEOS-5/GOCART system has also been used to investigate the impact of aerosols on tropical cyclones (Reale *et al*., 2011, 2014), aerosol semi-direct effects (Randles *et al*., 2013), Indian Monsoon (Kishcha *et al*., 2014, Yi *et al*., 2014), Saharan dust transport (Wong *at al*., 2008, Nowottnick *et al*., 2011, Colarco *et al*. 2013), and the aerosol impact on snow albedo (Yasunari *et al*., 2011,2014)

6. Carbon Species

In addition to aerosol species, GEOS-5 simulates the emission, uptake and transport of carbon monoxide (CO) and carbon dioxide (CO_2). A simplified version of CO chemistry, described in Ott et al. (2010), is used to increase computational efficiency. CO is emitted from biomass burning (Section 7.2), fossil and bio-fuel (section 7.2) combustion, and produced chemically from biogenic hydrocarbon and methane oxidation. CO emissions from fossil fuels, biofuels, and biomass burning are increased by 20%, 19%, and 11%, respectively, in order to account for CO production from non-methane hydrocarbons emitted from these sources. Biogenic isoprene and monoterpene emissions were calculated by the Global Modeling Initiative (GMI: Rotman *et al*., 2001) combined troposphere-stratosphere chemical transport model (CTM) using the method of Guenther *et al*. (1995) and are released directly as CO after applying an estimated yield during the oxidation of these species following Duncan *et al*. (2007). Monthly mean methane fields are used to calculate CO produced by methane oxidation as described in Bian *et al*. (2007). In order to calculate CO loss through reaction with OH, monthly mean OH fields produced by the GMI CTM for the year 2006 are used along with a prescribed loss frequency for CO.

CO_2 is also emitted by fossil fuel combustion and biomass burning. Natural fluxes of CO_2 between the atmosphere and land and ocean carbon reservoirs, calculated as part of NASA's Carbon Monitoring System (CMS) Flux Pilot Project (Ott *et al*., 2014, in review), are also included. Monthly net primary production (NEP) and ecosystem respiration were computed using the Carnegie-Ames-Stanford-Approach – Global Fire Emissions Database version 3 (CASA-GFED3) model (Randerson *et al*., 2013) and disaggregated to daily time intervals following Olsen and Randerson (2004). NEP fluxes, initially provided at 0.5-degree spatial resolution, were downscaled to 0.1 degree for the Nature Run by assuming that GPP is proportional to MODIS Enhanced Vegetation Index (EVI; Huete *et al*., 2002), a measure of vegetation greenness. Ecosystem respiration is downscaled by first assuming that, if vegetation is present in a 0.5 degree grid cell, heterotrophic and autotrophic contributions are of equal magnitudes. Autotrophic respiration is then assumed to be proportional to EVI while heterotrophic respiration is distributed uniformly across all land grid cells within the 0.5° grid box. In cells where no vegetation is present, all respiration is distributed uniformly across all land grid cells. Following the spatial downscaling, daily NPP and respiration are downscaled to three-hour periods following Olsen and Randerson (2004) to ensure a realistic diurnal cycle in atmospheric CO_2. Ocean CO_2 fluxes are calculated online in GEOS-5 following Wanninkhof (1992) using as input daily ocean surface partial pressure of CO_2 and salinity from NASA's Ocean Biogeochemical Model (NOBM; Gregg *et al*., 2003); sea surface temperatures (Reynolds *et al*., 2007); and GEOS-5 atmospheric CO_2 mixing ratios and 10-meter wind speeds.

7. Boundary Conditions and External Datasets

7.1 Sea-surface Temperature and Sea-Ice

Sea surface temperature and sea-ice are derived at ¼-degree from a combined Reynolds (Reynolds., 2007) OSTIA (Donlon *et al*., 2011) blended product. These daily SSTs are interpolated to the 7-km cubed-sphere grid and the data ocean component of GEOS-5 is called on the 30-minute radiation time-step.

7.2 Land surface boundary conditions

Mosaic land cover classes on the 7-km cubed-sphere grid (c1440) catchment-tiles were derived using 1km SiB2 land classification data from the USGS Global Land Cover Characteristics Data Base Version 2.0. Soil texture classes were derived using global data from the 5 arc-minute NGDC (National Geophysical Data Center) soil data (Reynolds *et al*., 1999). For each texture class, corresponding Cosby et al. soil hydraulic parameters were obtained from the second Global Soil Wetness Project (GSWP-2). Vegetation Parameters were derived from 1-degree GSWP-2 Leaf Area Index (LAI) and Greenness Fraction data were interpolated to c1440 catchment-tiles. 8-day Climatological cycles of diffused visible and diffused near-infrared albedo were computed using 30 arc-second MODIS (v5) data from the period 2001-2011. We scale model albedo to match the 8-day MODIS albedo climatology. Hydrologic catchment delineation data from HYDRO-1k were used to define c1440 catchment-tiles. The statistics of compound topography on each hydrologic catchment were also computed using HYDRO1k data.

7.3 Biomass Burning Emissions

Emissions of organic carbon (OC), black carbon (BC), sulfur dioxide (SO_2), carbon monoxide (CO) and carbon dioxide (CO2) from biomass burning are obtained from the Quick Fire Emissions Dataset (QFED) version 2.4-r6. The QFED is based on the fire radiative power (top-down) approach and draws on the cloud correction method used in the Global Fire Assimilation System (GFAS, Kaiser *et al*. (2012)) but in addition it employs a more sophisticated treatment of emissions from non-observed land areas (Darmenov and da Silva, 2014). Location and fire radiative power of fires are obtained from the Moderate Resolution

Figure 4. Seasonal mean QFED emissions of black carbon (BC µg m^{-2} s^{-1}) in 2006.

Imaging Spectroradiometer (MODIS) Level 2 fire products and the MODIS Geolocation products. Data from the Level 2 fire products are gridded at 0.1×0.1 degrees horizontal resolution and combined to create daily mean emissions at the same resolution. A diurnal cycle is imposed online on the daily mean emission values that is more prominent in the tropics and gradually weakens at higher latitudes in the North hemisphere's temperate zone. Seasonal mean biomass burning emissions of black carbon from the 0.5×0.5 degrees model output are shown in Figure 4. Spatial and temporal patterns of OC, SO_2, CO and CO_2 emissions are similar to the patterns of the BC emissions and are not shown here.
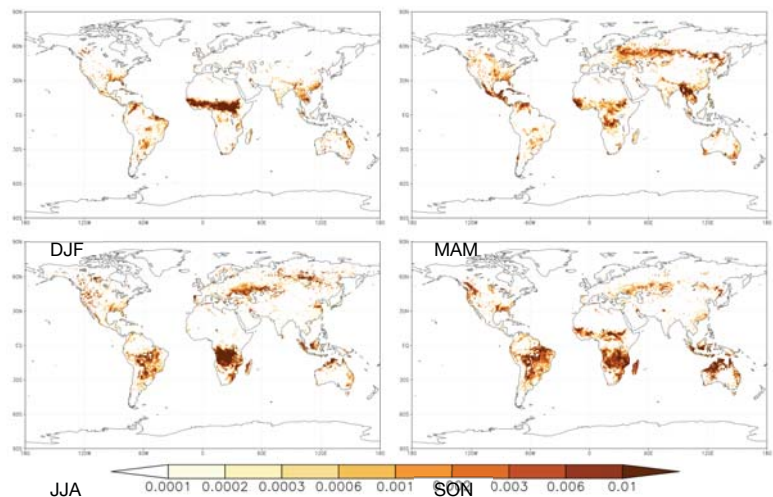
7.4 Anthropogenic Emissions

Anthropogenic emissions of carbon species and aerosols are largely taken from the Emissions Database for Global Atmospheric Research (EDGAR; Olivier *et al.*, 1994; EDGAR Project Team, 2009), which are provided annually at 0.1-degree resolution. For CO and CO_2, EDGAR v4.2 emissions from 2005 through 2007 were used in 7-km G5NR. CO emissions are temporally disaggregated from yearly to monthly using information on the seasonal cycle of fossil fuel emissions from Bey *et al.* (2001) while CO_2 fossil fuel seasonal cycles are imposed based on estimates from the Carbon Dioxide Information Analysis Center (CDIAC; Boden *et al.*, 2013).

For organic and black carbon aerosol species, which are not included in EDGAR v4.2, EDGAR-HTAP emissions were used in the Nature Run. To ensure consistency with previous GEOS-5 simulations, which have used emissions from the Aerosol Comparisons between Observations and Models (AeroCom; Myhre *et al.*, 2013) Phase II project, emission totals over 1-degree areas are adjusted to match yearly AeroCom emissions estimates for 2004 through 2008. Because EDGAR aerosol emissions are currently only available through 2005, the 2005 spatial distribution of EDGAR emissions are used to estimate Nature Run emissions in all years. The resulting anthropogenic emissions can be thought of as a hybrid between the EDGAR and AeroCom emissions datasets used, drawing information on total emissions and interannual variability from AeroCom while using EDGAR to achieve a high spatial resolution. SO_2 and SO_4 emissions from ships are handled similarly, by combining EDGAR and AeroCom emissions. Non-shipping emissions of SO_2 are taken directly from EDGAR v4.1 estimates for 2005 because of errors in AeroCom emissions discussed in Diehl *et al.* (2012).

7.5 Oxidant Fields

The GOCART tropospheric sulfate chemistry mechanism includes gas-phase and aqueous-phase reactions that account for the major chemical production and loss pathways of SO_2 and SO_4. Concentrations of hydroxyl radical (OH), nitrate radical (NO_3) and hydrogen peroxide (H_2O_2) are prescribed using monthly mean constituent fields from the NASA Global Modeling Initiative (GMI), (Duncan *et al.*, 2007; Strahan *et al.*, 2007) GMI-MERRA simulation. The GMI-MERRA simulation (Strahan *et al.*, 2013) was performed with the GMI chemical transport model, driven by assimilated meteorological data from MERRA, using an online parameterization of lightning NO_x emissions, specified biogenic VOC emissions, and biomass burning emissions from the GFED-v2 inventory (van der Werf *et al.*, 2006). Globally anthropogenic emissions were obtained from the EDGAR inventory. Over the Unites states, Europe and Asia the EDGAR emissions were augmented with emissions from the EPA NEI99, EMEP and the Streets inventory for 2006 (Zhang *et al.*, 2009), respectively. Diurnal variations of OH concentrations are computed by scaling the monthly mean fields to the cosine of the solar zenith angle. Diurnal variations of NO_3 are imposed by assuming zero concentrations in daylight and distributing the monthly mean values over night-time only. Because H_2O_2 is the limiting agent of the aqueous phase formation of SO_4 it is periodically reset every three hours to the monthly varying values. Prescribed monthly mean values of methane (CH_4) and OH, from a GMI simulation, are also used to calculate the chemical production and loss of CO.

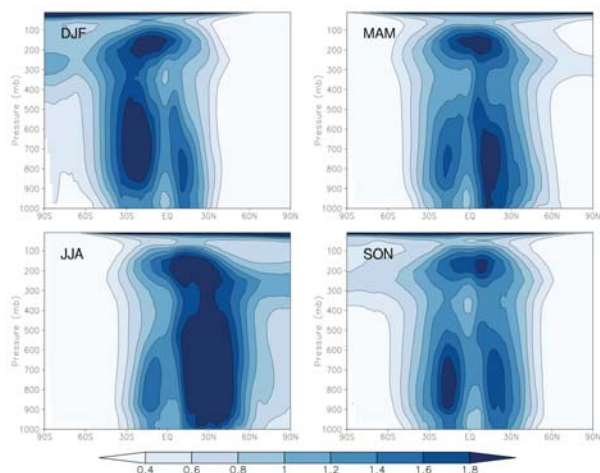**Figure 5. Zonal mean concentration (10^6 × molecules cm^{-3}) of hydroxyl radical (OH).**
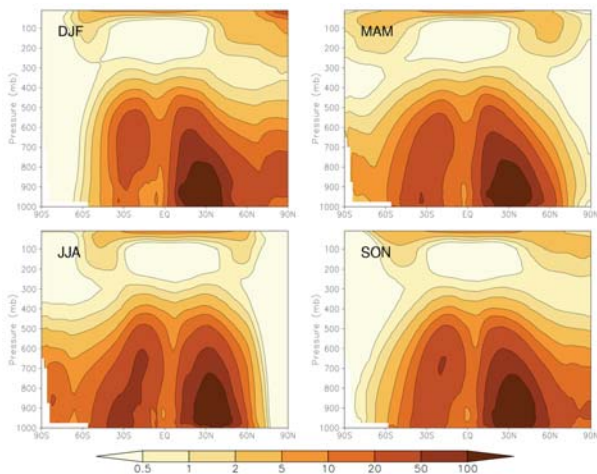

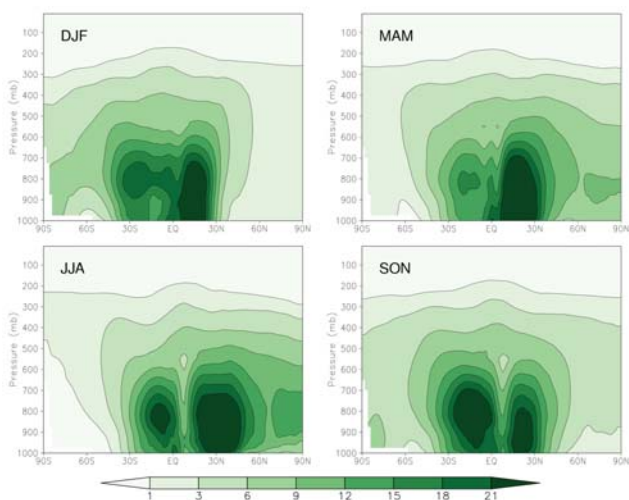**Figure 6. Zonal mean concentration (10^6 × molecules cm^{-3}) of nitrate radical (NO_3).**

Figure 7. Zonal mean concentration (10^9 × molecules cm^{-3}) of hydrogen peroxide (H_2O_2).

10

References

Bacmeister, J. T., M. J. Suarez, and F. R. Robertson, 2006: Rain Re-evaporation, Boundary Layer Convection Interactions, and Pacific Rainfall Patterns in an AGCM. *J. Atmos. Sci.*, **63**, 3383-3403.

Bey, I., D. J. Jacob, R. M. Yantosca, J. A. Logan, B. D. Field, A. M. Fiore, Q. Li, H. Liu, L. J. Mickley, and M. Schultz, 2001: Global modeling of tropospheric chemistry with assimilated meteorology: Model description and evaluation. *J. Geophys. Res.*, **106**, 23,073–23,095.

Bian, H., M. Chin, S. R. Kawa, B. Duncan, A. Arellano, and P. Kasibhatla, 2007: Sensitivity of global CO simulations to uncertainties in biomass burning sources. *J. Geophys. Res.*, **112**, doi:10.1029/2006JD008376.

Bloom, S., L. Takacs, A. da Silva, and D. Ledvina, 1996: Data assimilation using incremental analysis updates. *Mon. Wea. Rev.*, **124**, 1256-1271.

Boden, T.A., G. Marland, and R.J. Andres, 2013: Global, Regional, and National Fossil-Fuel CO_2 Emissions. Carbon Dioxide Information Analysis Center, Oak Ridge National Laboratory, U.S. Department of Energy, Oak Ridge, Tenn., U.S.A. doi:10.3334/CDIAC/00001_V2013.

Carpenter, R. L., K. K. Drogemeier, P. R. Woodward, and C. E. Hane, 1990: Application of the piecewise parabolic method to meteorological modeling. Mon. weather Rev., 118, 586-612.

Chou, M.-D., 1990: Parameterizations for the absorption of solar radiation by O_2 and CO_2 with applications to climate studies. *J. Climate*, **3**, 209-217.

Chou, M.-D., 1992: A solar radiation model for use in climate studies. *J. Atmos. Sci.*, **49**, 762-772.

Chou, M. -D., and M.J. Suarez, 1994: An efficient thermal infrared radiation parameterization for use in general circulation models, NASA Tech. Memorandum 104606-Vol 3, NASA, Goddard Space Flight Center, Greenbelt, MD.

Collins, N., G. Theurich, C. DeLuca, M. Suarez, A. Trayanov, V. Balaji, P. Li, W. Yang, C. Hill, and A. da Silva, 2005: Design and implementation of components in the Earth System Modeling Framework. *Int. J. High Perf. Comput. Appl.*, **19**, 341-350, DOI: 10.1177/1094342005056120.

Cullather, R.I., S.M.J. Nowicki, B. Zhao, and M.J. Suarez, 2014. Evaluation of the surface representation of the Greenland Ice Sheet in a general circulation model. J. Climate, 27, 4835-4856, doi:10.1175/JCLI-D-13-00635.1

Darmenov, A. and A. da Silva. The Quick Fire Emissions Dataset (QFED) - Documentation of versions 2.1, 2.2 and 2.4, NASA Tech. Memorandum (in preparation).

Derber, J. C., R. J. Purser, W.-S. Wu, R. Treadon, M. Pondeca, D. Parrish, and D. Kleist, 2003: Flow-dependent Jb in a global grid-point 3D-Var. *Proc. ECMWF annual seminar on recent developments in data assimilation for atmosphere and ocean.* Reading, UK, 8-12 Sept. 2003.

Diehl, T., A. Heil, M. Chin, X. Pan, D. Streets, M. Schultz, S. Kinne, 2012: Anthropogenic, biomass burning, and volcanic emissions of black carbon, organic carbon, and SO_2 from 1980 to 2010 for hindcast model experiments. *Atmos. Chem. Phys. Discuss.*, **12**, 24,895-24,954.

Donlon, C. J., M. Martin, J. D. Stark, J. Roberts-Jones, E. Fiedler and W. Wimmer, 2011. The Operational Sea Surface Temperature and Sea Ice analysis (OSTIA). *Remote Sensing of the Environment.* doi: 10.1016/j.rse.2010.10.017 2011.

Duncan, B. N., S.E. Strahan, Y. Yoshida, S.D. Steenrod, and N. Livesey, 2007: Model study of the cross-tropopause transport of biomass burning pollution, Atmos. Chem. Phys., 7, 3713–3736, doi:10.5194/acp-7-3713-2007.

Duncan, B. N., J. A. Logan, I. Bey, I. A. Megretskaia, R. M. Yantosca, P. C. Novelli, N. B. Jones, and C. P. Rinsland, 2007: Global budget of CO, 1988–1997: Source estimates and validation

with a global model. *J. Geophys. Res.,* **112**, doi:10.1029/2007JD008459.

Duynkerke, P., and S. de Roode, 2001: Surface energy balance and turbulence characteristics observed at the SHEBA Ice Camp during FIRE III. *J. Geophys. Res.*, **106**, 15313–15322, doi:10.1029/2000JD900537

EDGAR Project Team, 2009: Emission Database for Global Atmospheric Research (EDGAR), release version 4.0. http://edgar.jrc.ec.europa.eu. Eur. Comm. Joint Res. Cent., Brussels.

Errico, R. M., R. Yang, N. Privé, K.-S. Tai, R. Todling, M. Sienkiewicz, and J. Guo, 2013: Development and validation of observing-system simulation experiments at NASA's Global Modeling and Assimilation Office. *Q. J. Roy. Meteor. Soc*, **139**, 1162-1178. doi: 10.1002/qj2027

Garcia, R. R., and B. A. Boville, 1994: Downward control of the mean meridional circulation and temperature distribution of the polar winter stratosphere. *J. Atmos. Sci.*, **51**, 2238–2245.

Garfinkel, C.I., A. Molod, L. D. Oman and I.-S. Song, 2011: Improvement of the GEOS-5 AGCM upon Updating the Air-Sea Roughness Parameterization. *Geophys. Res. Lett.*, **38**, L18702, doi:10.1029/2011GL048802.

Godunov, S. K., 1959: Finite-difference methods for the numerical computations of equations of gas dynamics. *Math. Sb.*, **7**, 271–290

Gregg, W. W., P. Ginoux, P. S. Schopf, N. W. Casey, 2003: Phytoplankton and Iron: Validation of a global three-dimensional ocean biogeochemical model. *Deep-Sea Research II,* **50**, 3143-3169.

Guenther, A., C. N. Hewitt, D. Erickson, R. Fall, C. Geron, T. Graedel, P. Harley, L. Klinger, M. Lerdau, W. A. McKay, T. Pierce, B. Scholes, R. Steinbracher, R. Tallamraju, J. Taylor, and P. Zimmerman, 1995: A global model of natural volatile organic compound emissions. *J. Geophys. Res.,* **100**, 8873–8892.

Helfand, H. M., M. and S. D. Schubert, 1995: Climatology of the Simulated Great Plains Low-Level Jet and Its contribution to the Continental Moisture Budget of the United States. *J. Climate*, **8**, 784-806.

Hill, C., DeLuca, C., Balaji, V., Suarez, M., da Silva, A. and the ESMF Joint Specification Team, 2004: The Architecture of the Earth System Modeling Framework. IEEE Computing in Science and Engineering, "Grand Challenges in Earth System Modeling", **6**, No. 1, 18-28.

Huete, A., K. Didan, T. Miura, E. P. Rodriguez, X. Gao, and L. G. Ferreira, 2002: Overview of the radiometric and biophysical performance of the MODIS vegetation indices, *Rem. Sens. Env.*, **83**, 195-213.

Huynh, H. T., 1996: Schemes and constraints for advection. *Proc. Fifth Int. Conf. on Numerical Methods in Fluid Dynamics*, Monterey, CA.

Kaiser, J. W., A. Heil, M. O. Andreae, A. Benedetti, N. Chubarova, L. Jones, J.-J. Morcrette, M. Razinger, M. G. Schultz, M. Suttie, and G. R. van der Werf, 2012: Biomass burning emissions estimated with a global fire assimilation system based on observed fire radiative power. Biogeosciences, 9(1):527–554, 2012. doi: 10.5194/bg-9-527-2012.

Kondo, J., 1975: Air-sea bulk transfer coefficients in diabatic conditions. *Boundary Layer Meteor.*, **9**, 91-112.

Koster, R. D., M. J. Suárez, A. Ducharne, M. Stieglitz, and P. Kumar, 2000: A catchment-based approach to modeling land surface processes in a GCM, Part 1, Model Structure. *J. Geophys. Res.*, **105**, 24809-24822.

Large, W. G., and S. Pond, 1981: Open ocean momentum flux measurements in moderate to strong winds. *J. Phys. Oceanogr.*, **11**, 324-336.

Lin, S.-J. and R.B. Rood, 1996: Multidimensional flux-form semi-Lagrangian transport scheme. *Mon. Wea. Rev.,* **124**, 2046–2070

Lin, S.-J. and R.B. Rood, 1997: An explicit flux-form semi-Lagrangian shallow-water model on the sphere. *Q. J. R. Meteorol. Soc.*, **123**, 2477–2498

Lin, S.-J. and R.B. Rood, 1998: A flux-form semi-Lagrangian general circulation model with a Lagrangian control-volume vertical coordinate. *Proc. the Rossby-100 Symp., Stockholm, Sweden*, University of Stockholm, Sweden, 220–222.

Lin, S.-J., and R.B. Rood, 1999: Development of the joint NASA/NCAR General Circulation Model. Preprints, 13th Conf. on Numerical Weather Prediction, Denver, CO, Amer. Meteor. Soc., 115–119

Lin, S.-J., 2004: A 'vertically Lagrangian' finite-volume dynamical core for global models. *Mon. Wea. Rev.*, **132**, 2293–2307

Lock, A. P., A. R. Brown, M. R. Bush, G. M. Martin, and R. N. B. Smith, 2000: A new boundary layer mixing scheme. Part I: Scheme description and single-column model tests. *Mon. Wea. Rev.*, **138**, 3187–3199.

Louis, J. E, 1979: A Parametric Model of Vertical Eddy Fluxes in the Atmosphere, *Bound. Lay. Meteorol.*, **17**, 187-202

Louis, J. and J. Geleyn, 1982: A short history of the PBL parameterization at ECMWF. Proc. ECMWF Workshop on Planetary Boundary Layer Parameterization, Reading, United Kingdom, ECMWF, 59–80.

McFarlane, N. A., 1987: The effect of orographically excited gravity-wave drag on the circulation of the lower stratosphere and troposphere. *J. Atmos. Sci.*, **44**, 1775--1800.

Molod, A., 2012: Constraints on the Profiles of Total Water PDF in AGCMs from AIRS and a High-Resolution Model. *J. Climate*, **25**, 8341–8352.

Molod, A., L. Takacs, M.J. Suarez, J. Bacmeister, I.S. Song, A. Eichmann, and Y. Chang, 2011: The GEOS-5 Atmospheric General Circulation Model: Mean Climate and Development from MERRA to Fortuna. *Technical Report Series on Global Modeling and Data Assimilation 104606*, **v28**.

Molod, A., M. Suarez and G. Partyka, 2013: The impact of limiting ocean roughness on GEOS-5 AGCM tropical cyclone forecasts. *Geophys. Res. Lett.*, **40**, 411-415. DOI: 10.1029/2012GL053979

Moorthi, S., and M. J. Suarez, 1992: Relaxed Arakawa Schubert: A parameterization of moist convection for general circulation models. *Mon. Wea. Rev.*, **120**, 978-1002.

Myhre, G., B. H. Samset, M. Schulz, Y. Balkanski, S. Bauer, T. K. Berntsen, H. Bian, N. Bellouin, M. Chin, T. Diehl, R. C. Easter, J. Feichter, S. J. Ghan, D. Hauglustaine, T. Iversen, S. Kinne, A. Kirkevag, J.-F. Lamarque, G. Lin, X. Liu, M. T. Lund, G. Luo, X. Ma, T. van Noije, J. E. Penner, P. J. Rasch, A. Ruiz, O. Seland, R. B. Skeie, P. Stier, T. Takemura, K. Tsigaridis, P. Wang, Z. Wang, L. Xu, H. Yu, F. Yu, J.-H. Yoon, K. Zhang, H. Zhang, and C. Zhou, 2013: Radiative forcing of the direct aerosol effect from AeroCom Phase II simulations. *Atmos. Chem. Phys.*, **13**, 1853-1877.

Olivier, J., A. Bouwman, C. Maas, and J. Berdowski, 1994: Emission Database for Global Atmospheric Research (EDGAR). *Environ. Monit. Assess.*, **31**, 93-106.

Olsen, S. C., and J. T. Randerson, 2004: Differences between surface and column atmospheric CO_2 and implications for carbon cycle research. *J. Geophys. Res.,* **109**, doi:10.1029/2003JD003968.

Ott, L., B. Duncan, S. Pawson, P. Colarco, M. Chin, C. Randles, T. Diehl and J.E. Nielsen, 2010: Influence of the 2006 Indonesian biomass burning aerosols on tropical dynamics studied with the GEOS-5 AGCM. *J. Geophys. Res.,* **115***, doi:10.1029/2009JD013181.*

Ott, L. E., S. Pawson, G. J. Collatz, W. Gregg, D. Menemenlis, H. Brix, C. Rousseaux, K. Bowman, J. Liu, A. Eldering, M. Gunson, and S. R. Kawa, 2014: Quantifying the observability of CO_2 flux uncertainty in atmospheric CO_2 records using products from NASA's Carbon

Monitoring Flux Pilot Project, in review for *J. Geophys. Res.*

Putman, W. M. and S.-J. Lin, 2007: Finite-volume transport on various cubed-sphere grids. *J. Comput. Phys.,* **227**, 55-78.

Putman W. M., and S.-J. Lin, 2009: A finite-volume dynamical core on the cubed-sphere grid. Preprints, Numerical Modeling of Space Plasma Flows: ASTRONUM-2008, Astronomical Society of the Pacific Conference Series, vol 406, pp 268-276

Putman, W. M., and M. Suarez, 2011: Cloud-system resolving simulations with the NASA Goddard Earth Observing System global atmospheric model (GEOS-5), *Geophys. Res. Lett.*, 38, L16809, doi:10.1029/2011GL048438.

Pfafstetter, O., 1989: Classification of hydrographic basins: coding methodology, unpublished manuscript, Departamento Nacional de Obras de Saneamento, August 18, 1989, Rio de Janeiro; available from J.P. Verdin, U.S. Geological Survey, EROS Data Center, Sioux Falls, South Dakota 57198 USA. See, for example: Verdin, K.L. and J.P. Verdin, 1999: A topological system for delineation and codification of the Earth's river basins, *Journal of Hydrology*, vol. 218, nos. 1-2, pp. 1-12 or http://gis.esri.com/library/userconf/proc01/professional/papers/pap1008/p1008.htm

Randerson, J.T., G.R. van der Werf, L. Giglio, G.J. Collatz, and P.S. Kasibhatla. 2013. Global Fire Emissions Database, Version 3 (GFEDv3.1). Data set. Available on-line [http://daac.ornl.gov/] from Oak Ridge National Laboratory Distributed Active Archive Center, Oak Ridge, Tennessee, USA. doi:10.3334/ORNLDAAC/1191

Rasch, P. J., D. B. Coleman, N. Mahowald, D. L. Williamson, S-J. Lin, B. A. Boville, and P. Hess, 2006: Characteristics of atmospheric transport using three numerical formulations for atmospheric dynamics in a single GCM framework. *Journal of Climate*, **19(11)**, 2243-2266.

Reynolds, R. W., T. M. Smith, C. Liu, D. B. Chelton, K. S. Casey, and M. G. Schlax, 2007: Daily High-Resolution-Blended Analyses for Sea Surface Temperature. *J. Climate*, **20**, 5473–5496.

Rienecker, M.M., M.J. Suarez, R. Todling, J. Bacmeister, L. Takacs, H.-C. Liu, W. Gu, M. Sienkiewicz, R.D. Koster, R. Gelaro, I. Stajner, and J.E. Nielsen, 2008: The GEOS-5 Data Assimilation System - Documentation of Versions 5.0.1, 5.1.0, and 5.2.0. *Technical Report Series on Global Modeling and Data Assimilation 104606*, **v27**.

Rotman, D. A., J. R. Tannahill, D. E. Kinnison, P. S. Connell, D. Bergmann, D. Proctor, J. M. Rodriguez, S. J. Lin, R. B. Rood, M. J. Prather, P. J. Rasch, D. B. Considine, R. Ramaroson, and S. R. Kawa, 2001: Global Modeling Initiative assessment model: Model description, integration, and testing of the transport shell. *J. Geophys. Res.*, **106**, 1669-1691.Stieglitz, M., A. Ducharne, R. D. Koster, and M. J. Suarez, 2001: The Impact of Detailed Snow Physics on the Simulation of Snowcover and Subsurface Thermodynamics at Continental Scales. *J. Hydromet.*, **2**, 228-242

Strahan, S. E., B. N. Duncan, and P. Hoor, 2007: Observationally derived transport diagnostics for the lowermost stratosphere and their application to the GMI chemistry and transport model (2007), Atmos. Chem. Phys., 7, 2435–2445.

Strahan, S. E., A. R. Douglass, and P. A. Newman, 2013: The contributions of chemistry and transport to low Arctic ozone in March 2011 derived from Aura MLS observations, J. Geophys. Res. Atmos., 118, 1563–1576, doi:10.1002/jgrd.50181.

Tokioka, T., K. Yamazaki, A. Kitoh, and T. Ose, 1988: The equatorial 30-60 day oscillation and the Arakawa-Schubert penetrative cumulus parameterization. *J. Meteor. Soc. Japan*, **66**, 883-901.

Van Leer, B., 1977: Towards the ultimate conservative difference scheme. Part IV: A new

approach to numerical convection. *J. Comput. Phys.*, **23**, 276–299

Wanninkhof, R., 1992: Relationship between wind speed and gas exchange over the ocean, *J. Geophys. Res.*, **97**, 7373–7382.

van der Werf, G. R., J.T. Randerson, L. Giglio, G.J. Collatz, P.S. Kasibhatla, and A.F. Arellano Jr.: Interannual variability in global biomass burning emissions from 1997 to 2004, Atmos. Chem. Phys., 6, 3423-3441, doi:10.5194/acp-6-3423-2006, 2006.

Woodward, P. R., and P. Colella, 1981: High resolution difference schemes for compressible gas dynamics. Lect. Notes Phys., **141**, 434–441

Woodward, P. R., and P. Colella, 1984: The numerical simulation of two-dimensional fluid flow with strong shocks. *J. Comput. Phys.*, **54**, 115–173

Wu, W.-S., R.J. Purser and D.F. Parrish, 2002: Three-dimensional variational analysis with spatially inhomogeneous covariances. *Mon. Wea. Rev.*, **130**, 2905-2916.

Zhang, Q., D.G. Streets, G.R. Carmichael, K.B. He,, H. Huo, A. Kannari, Z. Klimont, I.S. Park, S. Reddy, J.S. Fu, D. Chen, L. Duan, Y. Lei, L.T. Wang, and Z.L. Yao, 2009: Asian emissions in 2006 for the NASA INTEX-B mission, Atmos. Chem. Phys., 9, 5131-5153, doi:10.5194/acp-9-5131-2009.

Web Resources

GMAO web site: http://gmao.gsfc.nasa.gov/

NetCDF information: http://www.unidata.ucar.edu/software/netcdf/

CF Standard Description: http://cf-pcmdi.llnl.gov/

The HDF Group: http://www.hdfgroup.org /

Acronyms

ADAS	atmospheric data assimilation system
AOT	aerosol optical thickness
CF	Climate and Forecast metadata convention
CLSM	Catchment Land Surface Model
COARDS	Cooperative Ocean/Atmosphere Research Data Service metadata convention
DMS	dimethylsulphide
ECS	EOS Core System
EOS	Earth Observing System
ESDT	Earth Science Data Type
ESMF	Earth System Modeling Framework
FP	Forward-processing
GES DISC	Goddard Earth Sciences Data and Information Services Center
GMAO	Global Modeling and Assimilation Office
GRIB	GRIdded Binary
GSI	Gridpoint Statistical Interpolation
HDF	Hierarchical Data Format
IAU	Incremental Analysis Update
JCSDA	Joint Center for Satellite Data Assimilation
MSA	methane sulphonic acid
NCEP	National Center for Environmental Prediction
NetCDF	Network Common Data Form
PAR	photosynthetically active radiation
TOA	top of atmosphere
TOMS	Total Ozone Mapping Spectrometer
UTC	Universal Time, Coordinated

Appendix A: Vertical Structure

A.1 Hybrid Sigma-Pressure Levels

Products on the native vertical grid will be output on the following levels. Pressures are nominal for a 1000 hPa surface pressure and refer to the top edge of the layer. Note that the bottom layer has a nominal thickness of 15 hPa.

Lev	*P(hPa)*	*Lev*	*P(hPa)*	*Lev*	*P(hPa)*	*Lev*	*P(hPa)*	*Lev*	*P(hPa)*	*Lev*	*P(hPa)*
1	0.0100	13	0.6168	25	9.2929	37	78.5123	49	450.000	61	820.000
2	0.0200	14	0.7951	26	11.2769	38	92.3657	50	487.500	62	835.000
3	0.0327	15	1.0194	27	13.6434	39	108.663	51	525.000	63	850.000
4	0.0476	16	1.3005	28	16.4571	40	127.837	52	562.500	64	865.000
5	0.0660	17	1.6508	29	19.7916	41	150.393	53	600.000	65	880.000
6	0.0893	18	2.0850	30	23.7304	42	176.930	54	637.500	66	895.000
7	0.1197	19	2.6202	31	28.3678	43	208.152	55	675.000	67	910.000
8	0.1595	20	3.2764	32	33.8100	44	244.875	56	700.000	68	925.000
9	0.2113	21	4.0766	33	40.1754	45	288.083	57	725.000	69	940.000
10	0.2785	22	5.0468	34	47.6439	46	337.500	58	750.000	70	955.000
11	0.3650	23	6.2168	35	56.3879	47	375.000	59	775.000	71	970.000
12	0.4758	24	7.6198	36	66.6034	48	412.500	60	800.000	72	985.000

Appendix B: Surface Representation

In GEOS-5 the surface below each atmospheric column consists of a set of tiles that represent various surface types. Tiles can be of four different types: Ocean, Land, Ice, and Lake, as illustrated in Figure 8. In each grid box a single Ice tile represents those areas covered by permanent ice. Similarly a single Lake tile represents continental areas covered permanently by water. Other continental areas (non Lake or Ice) can be further subdivided into tiles that represent parts of the grid box in different hydrological catchments, defined according to the Pfafstetter (1989) system. Each of these is, in turn, divided into subtiles (not shown in figure 8) that represent the wilted, unsaturated, saturated, and snow-covered fractions of the tile. These fractions vary with time and are predicted by the model based on the hydrological state of the catchment and its fine-scale topographic statistics. Details of the land model, including the partitioning into subtiles, can be found in Koster *et al.* (2000). The Ocean tile can be divided into two subtiles that represent the ice-covered and ice-free parts of the ocean part of the atmospheric grid box. The fractional cover of these subtiles also varies with time.

Figure 8. Schematic of the Ocean, Land, Ice and Lake tiles used in the land-surface model, as described in Appendix B.

18